Journal of Materials Chemistry C

RSC Publishing

PAPER

View Article Online
View Journal | View Issue

Cite this: J. Mater. Chem. C, 2013, 1, 1383

The structural, optical and electrical characterization of high-performance, low-temperature and solution-processed alkali metal-doped ZnO TFTs†

Si Yun Park,[a] Kyongjun Kim,[a] Keon-Hee Lim,[a] Beom joon Kim,[b] Eungkyu Lee,[a] Jeong Ho Cho[b] and Youn Sang Kim*[ac]

Received 5th November 2012
Accepted 11th December 2012

DOI: 10.1039/c2tc00559j

www.rsc.org/MaterialsC

The structural, electrical and optical properties of high-performance, low-temperature and solution-processed alkali metal-doped ZnO TFTs were studied using various analytic instruments, including HR-TEM, AFM, XPS, EDS, electrical bias stability test and UV-vis spectroscopy. Furthermore, we successfully demonstrated that a change in the optical bandgap energy of Li-doped ZnO semiconductor films supported by Burstein–Moss theory can show a trade-off relationship between the field effect mobility of Li-ZnO TFTs and the Li doping concentrations. The relative broadening of the E_{opt} values, which are strongly related to the amount of excited electrons from the Fermi level in the valance band to the conduction band, was observed from the undoped ZnO film to the Li-doped ZnO film (10 mol%). The increase in the electron donor concentration was the dominant reason for the enhancement in the electron mobility of the alkali metal-doped ZnO TFTs.

1 Introduction

Transparency and flexibility are new terms of innovation associated with advanced display applications such as head-up displays for cars, smart windows, display tables, smart cards and rollable smart phones. Hence, thin film transistors (TFTs) as a driving element in devices that utilize an active matrix display require not only semiconductors that are capable of high level of performance but also unique materials properties such as transparency. Moreover, advanced process conditions are required, such as a low-temperature sintering for flexible devices on a plastic substrate and solution-processibility for low cost and large-area manufacturing.[1]

Recently, TFTs based on metal oxide semiconductors, such as In, Ga and Zn oxides, have garnered a considerable amount of interest owing to their valuable performance characteristics, such as their high electron mobility and large on/off current ratio, as compared to other semiconductors.[2] Also, as metal oxide semiconductors have a wide bandgap with a large exciton binding energy,[3] they have a good transmittance and are quite stable in air.[4] Given these outstanding characteristics, TFTs based on metal oxide semiconductors are now excellent candidates for switching devices in next-generation displays.

In general, to apply them for the semiconductor in a TFT, metal oxide semiconductors have been deposited as films on substrates using various vacuum techniques, such as pulsed laser deposition (PLD),[5] radio frequency (RF) sputtering,[6] metal–organic chemical vapour deposition (MOCVD)[7] and atomic layer deposition (ALD),[8] all of which ensured outstanding electrical performance. For example, Fortunato *et al.* reported that amorphous indium zinc oxide (IZO) TFTs fabricated by RF sputtering showed an excellent field effect mobility, which was better than that of conventional amorphous silicon TFTs by one hundred times or even better than the performance of general polycrystalline silicon TFTs.[9] In addition, Hosono *et al.* successfully demonstrated the flexible TFTs with a high field effect mobility of $\sim$7 $cm^2\ V^{-1}\ s^{-1}$ using amorphous In–Ga–Zn–O (indium–gallium–zinc–oxide, IGZO) semiconductors fabricated by PLD.[10] As the field electron mobility for applications of display devices such as OLEDs requires over $\sim$5 $cm^2\ V^{-1}\ s^{-1}$, metal oxide TFTs have good potential for use as switching devices in advanced displays.[11]

Despite these remarkable electrical features, batch-type vacuum deposition processes such as PLD, RF sputtering, MOCVD and ALD continue to have fundamental problems in that they require high facility investment levels. Solution processibility in ambient conditions is essential for an advanced device fabrication process to achieve low-cost and

[a]Program in Nano Science and Technology, Graduate School of Convergence Science and Technology, Seoul National University, 864-1 Iui-dong, Yeongtong-gu, Suwon-si, Gyeonggi-do 443-720, Republic of Korea. E-mail: younskim@snu.ac.kr; Fax: +82-31-888-9148; Tel: +82-33-888-9131

[b]SKKU Advanced Institute of Nanotechnology (SAINT), Sungkyunkwan University, Suwon-si, Gyeonggi-do 440-746, Republic of Korea. E-mail: jhcho94@gmail.com

[c]Advanced institutes of convergence technology, 864-1 Iui-dong, Yeongtong-gu, Suwon-si, Gyeonggi-do 443-270, Republic of Korea

† Electronic supplementary information (ESI) available: The electrical characteristics of ZnO-TFTs with various doping concentrations, the method of calculating the optical bandgap, TGA, XPS and EDS data for ZnO thin films. See DOI: 10.1039/c2tc00559j

large-area manufacturing. Also, for application to flexible devices, a low-temperature process is an important element. Furthermore, in addition to these requirements, the prerequisite of indium, which is scarce but a strategically important material, is a challenge to be solved.

Solution processes such as drop-cast, spin-cast, ink-jet printing processes can be applied with soluble metal oxide precursors or nanoparticles dispersed in a solvent.[12,13] Keszler *et al.* reported stable precursor inks based on ammine-hydroxo zinc species. These were transformed to polycrystalline ZnO for active layers of TFTs after annealing at a very low temperature of ~150 °C, and showed a field effect mobility of ~0.4 $cm^2 V^{-1} s^{-1}$.[14] Recently, we reported newly the ZnO semiconductor precursors for the active channel of transistors, which is based on an ammine-hydroxo zinc complex, without time-consuming purification steps and with a low annealing temperature as maximum as 300 °C,[15] and demonstrated the unique patterning technique for TFT arrays using this ZnO semiconductor precursor.[16] Although some noteworthy results have been reported for the low-temperature annealing and solution-processibility, intrinsic ZnO ink still shows relatively inferior electron mobility.

To enhance the electrical performance, various metal-alloy zinc oxides such as IZO and IGZO, which are still solution-processible, have been reported to compensate for the poor electrical performance of intrinsic ZnO semiconductors.[17,18] Although devices based on these metal-alloy oxide zinc semiconductors have shown good electrical performance capabilities, the massive use of indium (In) as a dopant causes some problems, which is becoming expensive and strategically important.

To address these issues, we previously introduced alkali metal dopants, particularly focused on lithium (Li) and sodium (Na), to fabricate the low-temperature and solution-processed ZnO TFTs which remarkably enhanced the field effect mobility values and on/off current ratio.[15] However, the exact mechanism and a detailed analysis of the alkali metal doping effects remain unavailable, which has undermined the good potential of alkali metal-doped metal oxide TFTs. Herein, we discussed the alkali metal doping effects on ZnO semiconductors in terms of its crystallinity, morphology, interface charge trapping, optical bandgap, XPS analysis and so on. In addition, we proved that alkali metals locate at the interstitial sites in the polycrystalline ZnO matrix and newly suggested that the enhancement of the field effect mobility of alkali metal-doped ZnO TFTs can be successfully explained in terms of changes in the optical properties using a spectroscopic analysis.

2 Results and discussion

In general, metal oxide semiconductor TFTs based on ZnO have shown field effect mobility values ranging from 0.2 to 50 $cm^2 V^{-1} s^{-1}$ depending on various process conditions, such as the deposition method, sintering temperature for crystallinity of the semiconductor and the interface control between the semiconductor and the insulator.[5,19,20] Single-crystalline ZnO semiconductor films are most favourable for TFTs capable of high electrical performance. However, to obtain high-quality single-crystalline ZnO films, a template substrate such as single-crystal (111) yttria-stabilized zirconia is essential to grow epitaxial ZnO thin layers, and they require a very high growth temperature (~700 °C).[21] Also, these single-crystalline ZnO semiconductors require a high-cost vacuum process such as MOCVD or PLD. These process conditions have seriously undetermined the good potential of metal oxide TFTs.

To extend the potential of ZnO TFTs to advanced displays, ZnO semiconductors require not only high electrical performance but also a low-temperature and solution-processible approach. Several previous reports have introduced polycrystalline ZnO TFTs through a low-temperature, solution-based process.[11,14] However, as the electrical performance of intrinsic polycrystalline ZnO semiconductors has not been good enough to meet the demands of advanced displays, considerable attention has been paid to various dopants to enhance the electrical performance, such as the electron mobility, on/off current ratio and reliability. In a previous report, we introduced a simple route to achieve high-performance, low-temperature and solution-processed ZnO TFTs by employing alkali metal doping with Li, Na, K or Rb.[15] The alkali metal-doped TFTs not only showed excellent performance but also allowed the rare and expensive indium (In) element to be omitted. In spite of the good potential of alkali metal-doped ZnO TFTs in our previous reports, many details that should be addressed, such as their low-temperature solution-processibility, their high mobility and their excellent operational stability, still remain. Initially, we investigated the correlation and dependence of the alkali metal doping concentration, the crystallinity and the morphology of alkali metal-doped ZnO semiconductors.

The alkali metal-doped ZnO thin films were prepared by spin-coating from mixtures of zinc ammonia and alkali metal hydroxides. Different molar ratios (1, 10, and 15 mol%) of alkali metal hydroxides, in this case lithium hydroxide (LiOH) and sodium hydroxide (NaOH), were added to the zinc ammonia solution. The as-coated films on silicon wafers (SiO_2/Si) were annealed at 300 °C on a hot plate under ambient conditions for 1 hour, forming alkali metal-doped ZnO semiconductor films. In order to examine the electrical performance of the alkali metal-doped ZnO, bottom gate-top contact ZnO TFTs with SiO_2 gate dielectrics were fabricated. The transfer curves and output curves of Li-doped ZnO TFTs showed typically a n-channel behaviour irrespective of doping concentration (see the ESI, Fig. S1†).

Fig. 1 shows cross-sectional HR-TEM images of Li-doped ZnO films with various doping concentrations (Li 0–15 mol%). The inset in Fig. 1c clearly shows crystalline FFT-SAED (Fast Fourier Transform Selected Area Electron Diffraction) patterns, showing that Li-doped ZnO films have a polycrystalline structure. In the image of the SAED pattern, although there was faint scattering induced by an amorphous SiO_2 dielectric layer, we could not observe any remarkable lattice distortion or migration caused by the lithium (Li) doping.[22] Fig. 2 shows the surface morphology changes in ZnO semiconductor films using an Atomic Force Microscope (AFM) at various Li doping

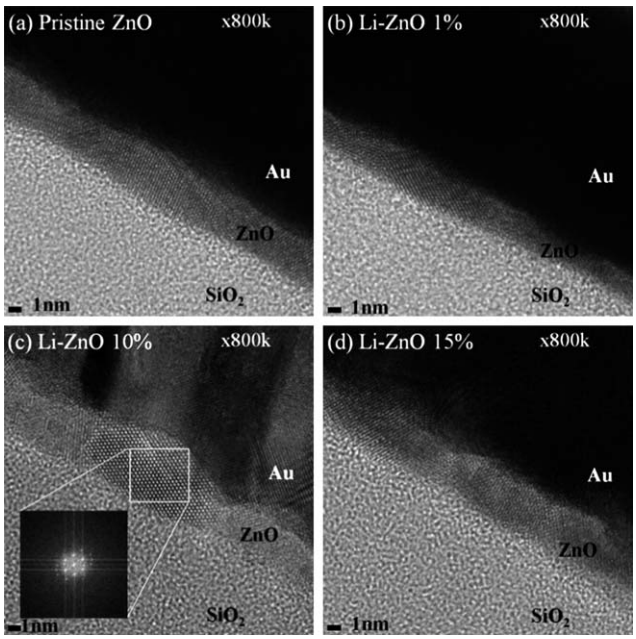

Fig. 1 Cross-sectional HR-TEM images of Li-doped ZnO films on the SiO_2 substrate at annealing temperature 300 °C. (a) Pristine ZnO film, (b) Li-doped ZnO film with 1 mol%, (c) Li-doped ZnO film with 10 mol% (the inset shows crystalline FFT-SAED patterns) and (d) Li-doped ZnO film with 15 mol%.

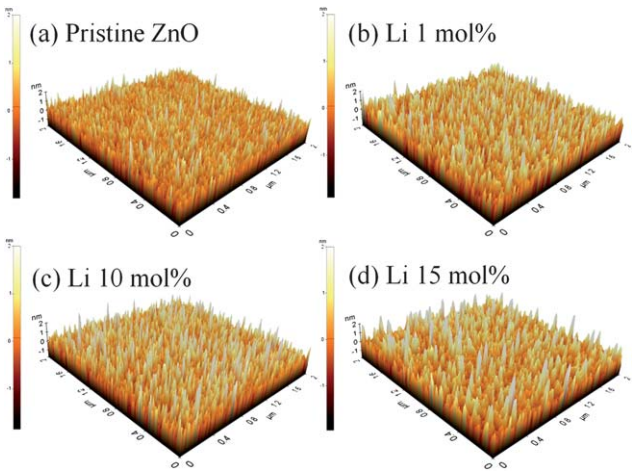

Fig. 2 Atomic force microscopy (AFM) images of Li-doped ZnO films. The root mean square (RMS) roughness values of ZnO films were 0.429 nm (pristine ZnO), 0.565 nm (Li 1 mol%), 0.587 nm (Li 10 mol%), and 0.524 nm (Li 15 mol%).

concentrations. The values of the root mean square (RMS) roughness were 0.429 nm (pristine ZnO film), 0.565 nm (Li-doped ZnO film with Li 1 mol%), 0.582 nm (Li-doped ZnO film with Li 10 mol%), and 0.587 nm (Li-doped ZnO film with Li 15 mol%).

The slight differences in the RMS roughness of the ZnO semiconductor films were attributed to an increase in the surface undulation as the Li concentration increased.[23] As the changes of the grain size in various ZnO films were too small, there did not seem to be any strong correlation with the enhancement in the electron mobility. The changes of the surface morphology and grain size could not be used to explain the variance in the electron mobility of ZnO TFTs depending on the alkali metal doping concentration, as remarkable changes in the ZnO morphology were not detected in the polycrystalline ZnO structure after the addition of alkali metal dopants. In spite of the investigation of a direct correlation between the morphology and crystallinity of ZnO semiconductor films and the electrical performance, in this study, we did not find any remarkable tendency. For a clear explanation of the electrical properties of alkali metal-doped ZnO semiconductor films, other analyses or mechanisms are required.

For the TFTs used in advanced displays such as active matrix OLEDs, a highly stable threshold voltage, ΔV_{th}, and no degradation of the field effect mobility during repeated operations are essential. Because active matrix OLEDs are current-dependent devices, the TFTs should work at a constant ΔV_{th}.[24] Preventing threshold voltage shifts and maintaining high field effect mobility values are critical issues in metal oxide TFTs when they are used as pixel switches in advanced displays. In general, the shift of the threshold voltage and field effect mobility during bias stress comes from defects in the semiconductor layer or trap in the interface between the semiconductor and the dielectric layer.[25] Through an investigation of the bias stability of ZnO TFTs, the charge trapping sites in the ZnO matrix or interface charge trapping between the ZnO semiconductor and dielectric layers could be elucidated. To exclude the shift of the threshold voltage and field effect mobility induced by chemical reaction and interface diffusion in ZnO semiconductors with ambient oxygen or moisture,[26] bias stability tests were carried out in a vacuum condition.

Fig. 3 shows the positive shift of the transfer curves depending on the operation time under positive bias stress. A strong gate bias (V_G) of 50 V was continuously applied under vacuum conditions for 6000 seconds. The relative threshold voltage shifts (ΔV_{th}) of TFTs fabricated with a ZnO semiconductor including Li 10 mol% and a pristine ZnO semiconductor as a reference are summarized in Fig. 3a and b, respectively. Remarkably, the threshold voltage shift in the Li-doped ZnO TFTs ($\Delta V_{th} = 1.67$ V) was much smaller than that in the pristine ZnO TFTs ($\Delta V_{th} = 6.24$ V). The improvement of ΔV_{th} could be understood in terms of the decrease in the interface defects induced from the Li doping in the ZnO matrix. In general, as solution-processed ZnO films have considerable numbers of intrinsic defects in spite of the completeness of the chemical reactions, pristine ZnO TFTs show a slight instability in their ΔV_{th} values. Otherwise, at the optimized doping of Li (10 mol%), the charge trapping sites in the ZnO matrix or the interfaces between the ZnO semiconductors and the dielectric layers were reduced by the efficient compensation of traps with Li interstitial doping. Previously, we reported an enhancement of the charge transport in a Li-doped ZnO semiconductor using an observation of the thermal activation energy of carrier hopping.[15] These results indicate that the charge trapping sites in the ZnO matrix can be reduced by Li doping in ZnO semiconductors. Furthermore, we think that the highly stable operation of Li-doped ZnO TFTs is attributed to the effectual offsetting of the interface traps with Li doping.

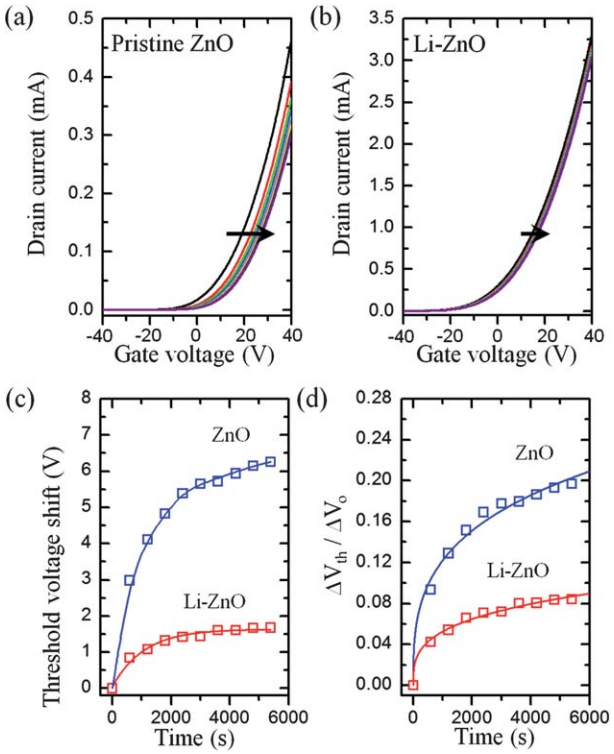

Fig. 3 (a) Evolution of the linear transfer curves of pristine ZnO TFTs, as a function of bias stress time (0–6000 s). (b) Evolution of the linear transfer curves of Li-doped ZnO TFTs (10 mol%), as a function of bias stress time (0–6000 s). (c) Relative threshold voltage shift (ΔV_{th}) of Li-doped ZnO TFTs (10 mol%) as a function of stress time. (d) Plot of $\Delta V_{th}/V_o$ *vs.* bias stress time for the pristine and Li-doped ZnO (10 mol%) TFTs. The solid curves were fit to a stretched exponential equation.

The electrical stability of ZnO TFTs was quantified by the modelling of the threshold voltage shift using the stretched exponential equation, as follows:[27]

$$\frac{\Delta V_{th}}{\Delta V_o} = \frac{V_{th} - V_{th,initial}}{V_g - V_{th,initial}} = 1 - \frac{1}{\left\{1 + \exp\left[\frac{(E_{th} - E_A)}{k_B T_0}\right]\right\}^{\frac{1}{(\alpha-1)}}} \quad (1)$$

$V_{th,initial}$ is the initial threshold voltage, E_A is the typical activation energy for trap creation, k_BT_0 is the slope of the activation energy distribution, and α is a constant. E_{th} corresponds to the thermalization energy, defined by $k_BT\ln(\nu t)$. Here, k_B, ν, T and t are the Boltzmann constant, the attempt-to-escape frequency, the temperature and the bias stress time, respectively. The curves of ΔV_{th} *vs.* the operation time in Fig. 3c successfully show the saturation of ΔV_{th}, which is a prerequisite of eqn (1).[28] Also, as the pristine and Li-doped ZnO TFTs in this approach have negligible hysteresis, we successfully calculated E_A and k_BT from the fitting parameters (E_A, k_BT_0, ν, and α) in Fig. 3d. The calculated parameters of ν and α were 1×10^5 Hz and 1.5, respectively.

These values were acceptable and reasonable, considering previously reported values.[27] The parameters related to the activation energy, *i.e.*, E_A and k_BT, varied depending on the Li dopant concentration, as summarized in Table 1. As a high activation energy for trap creation, E_A, in a semiconductor induces stable operation and a small value of ΔV_{th} when the device operates,[28] Li doping could efficiently improve the electrical stability of ZnO TFTs. We think that these reductions of ΔV_{th} values in Li-doped ZnO TFTs (Li 10 mol%) are attributed to interstitial doping of Li in the polycrystalline ZnO structure.

Table 1 E_A and k_BT_0 of pristine and Li-doped ZnO TFTs (10 mol%)

	Pristine ZnO	Li-ZnO (10 mol%)
E_A (eV)	0.679 (±0.013)	0.772 (±0.018)
k_BT_0 (eV)	0.075 (±0.006)	0.082 (±0.005)

Zinc oxide has the unique characteristic in which the injection of electron carriers can be achieved by chemical doping. In conventional crystalline materials such as silicon semiconductors, substitutional doping is a conventional phenomenon which serves to enhance the semiconductor properties from their intrinsic levels. However, in the ZnO semiconductor, as zinc ions have strong ionic bonding with oxygen and bonding has flexibility in the coordination structure, the doping mechanism is somewhat more complex than that of a conventional Si semiconductor. A p-type semiconductor property can be obtained when a considerable amount of lithium (Li) exists at substitutional sites in the ZnO matrix.[22] In such a case, lithium acts as an acceptor, which can lead to inversion p-channel ZnO TFT operation. However, Park *et al.* predicted that Li (or Na) in the ZnO matrix prefers basically interstitial sites to substitutional sites.[29] Also, Hosono *et al.* suggested the possibility of effective n-type doping in ZnO through the ion implantation of a cation that has low electron affinity.[30] If group-I elements occupy the interstitial sites, they act as a shallow donor.[29] Li in ZnO can occupy the interstitial site as well as the substitutional zinc site in the ZnO matrix. Eqn (2) and (3) explain the Li defect mechanism in ZnO.[31]

$$Li \rightarrow Li_i^+ + e^- \quad (2)$$

$$Li \rightarrow Li_{Zn} + h^+ \quad (3)$$

Li_{Zn} and Li_i^+ represent the lithium on the Zn lattice sites in the substitutional position and the lithium in the interstitial position on the lattice, respectively. Given that intrinsic ZnO is an n-type semiconductor that has donor electrons, the substitutional doping of Li neutralizes the carriers in the ZnO semiconductor and reduces the field effect mobility of ZnO TFTs. However, the interstitial doping can improve the carrier concentration by the increment of electrons. To investigate interstitial doping, we measured the optical bandgap using a UV-vis spectroscope. The optical bandgap energy, E_{opt}, can be calculated from the absorption coefficient (α). The α coefficient can be obtained by modified eqn (4), as follows (see the ESI†):

$$\alpha = \frac{1}{D}\ln\left(\frac{1}{T}\right) \quad (4)$$

D is the film thickness and T is the transmittance. The film thickness (D) of ZnO was ~7 nm. The optical bandgap E_{opt} is given by eqn (5), as follows:

$$(\alpha h\nu)^2 = A(h\nu - E_{opt}) \quad (5)$$

A is a constant and hv denotes the photon energy. Fig. 4a shows the transmission spectra of Li-doped ZnO films annealed at 300 °C in ambient air for 1 hour. All films have an average optical transparency that exceeds 90% in the visible wavelength range. The inset in Fig. 4a shows that the transmittance was elevated and then declined as the Li concentration increased. These results can be correlated with the change of the optical bandgap value.

Fig. 4b shows a plot of $(\alpha h\nu)^2$ *vs.* the photon energy in the various ZnO films; the E_{opt} value can be obtained by extrapolating the linear region to the photon energy axis. The detailed method of calculating the optical bandgap is provided in the ESI.† The optical bandgap energy values, E_{opt}, of Li-doped ZnO films were 3.24 eV (0 mol%), 3.28 eV (1 mol%), 3.31 eV (10 mol%), and 3.30 eV (15 mol%) (see Table 2).

The widening of the E_{opt} values was induced from the quantum confinement size effect (QSE). The QSE arises when the crystalline size of ZnO is similar to its Bohr exciton radius. Size dependence of the optical bandgap energy is clearly detected in the QSE regime when ZnO particles are smaller than 5 nm.[32] However, HR-TEM images show that the crystalline size of ZnO is far from the QSE regime. Thus, the increase and decrease in the E_{opt} values given various alkali metal dopant concentrations can be explained by Burstein–Moss effects. In keeping with Burstein–Moss effects, because a doubly occupied state is restricted by the Pauli principle and assuming that the optical transition is vertical, extra energy is required to excite valence electrons to higher states in the conduction band, which causes the widening of the optical bandgap.[33] The alkali metals located at the interstitial sites in the ZnO matrix cause an increase in the donor electrons (eqn (2)), and the widening optical bandgap is caused by excess donor electrons. When 10 mol% of lithium hydroxide was added, the Li-doped ZnO TFTs were highest in terms of field effect mobility (see Fig. 5).

Exceeding the optimum dopant concentration, both the field effect mobility and the optical bandgaps were reduced. Therefore, we assume that the majority of the alkali metal ions must exist as interstitial donors in the structure rather than as substitutional acceptors. The narrowing of the E_{opt} value from 3.31 eV to 3.30 eV can be explained by the substitutional doping of Li. When the Li concentration in the ZnO matrix exceeded 10 mol%, despite the interstitial doping that occurred, substitutional Li doping also occurred simultaneously and in considerable amounts. This substitutional doping of Li generated the electron acceptors (the holes) induced by Li at the substitutional sites (eqn (3)), which neutralized the electron donors induced by Li at the interstitial sites and decreased the field effect mobility of TFTs.

This trade-off phenomenon between the field effect mobility and the alkali metal dopant concentrations in ZnO semiconductors requires a more intensive study. However, in this study, the change of the optical bandgap energy in Li-doped ZnO semiconductors as supported by the Burstein–Moss theory successfully showed the increase and decrease of the field effect

Table 2 Optical bandgap of Li-doped ZnO films with different doping concentrations

Doping concentration (mol%)	Average of optical band gap (eV)
Pristine ZnO films	3.2638
Li-doped ZnO films (1 mol%)	3.2868
Li-doped ZnO films (10 mol%)	3.2973
Li-doped ZnO films (15 mol%)	3.2857

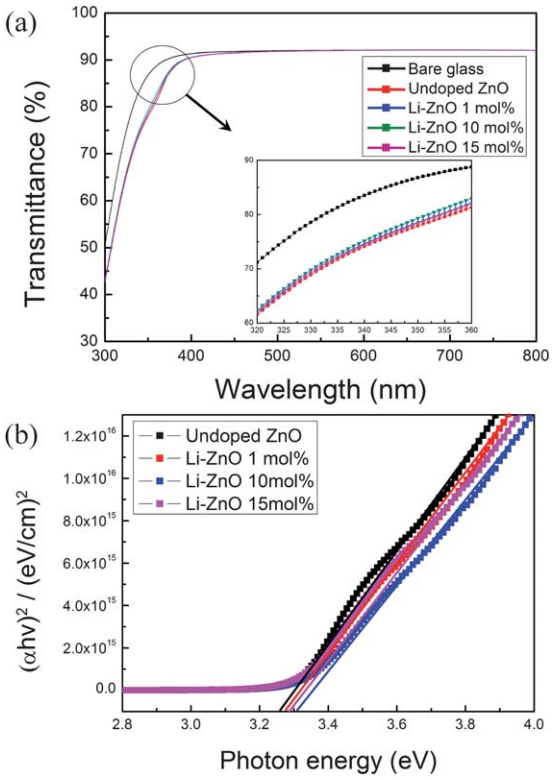

Fig. 4 (a) The optical transmittance spectrum of Li-doped ZnO films on the glass substrate. The inset shows that the transmittance was elevated and then declined with increasing Li concentration. (b) The $(\alpha h\nu)^2$ *vs.* photon energy plot of the Li-doped ZnO films with various doping concentrations (0, 1, 10 and 15 mol%). The box chart of optical band gap *vs.* Li doping concentration is shown in Fig. S2.†

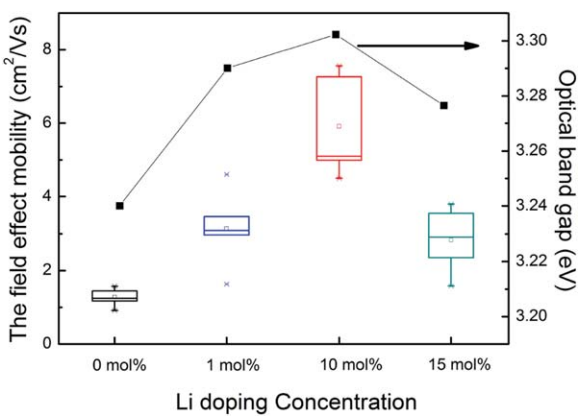

Fig. 5 The field effect mobility and optical band gap energy of Li-doped ZnO semiconductors with various doping concentrations (0, 1, 10 and 15 mol%).

mobility of Li-doped ZnO TFTs and the connection between this and the doping concentration of lithium (Li).

The shift of turn-on voltage of Li-doped ZnO TFTs can be observed in Fig. 6a. This phenomenon was related to the charge density in the ZnO semiconductor layer. The charge density in the channel layer, N_T, corresponding to the turn-on voltage, V_{on}, is approximately estimated as[34]

$$N_T = \frac{C_i V_{on}}{q t_c} \quad (6)$$

where C_i is the gate insulator capacitance per unit area, q is the elementary charge, and t_c is the thickness of the channel layer. The turn-on voltages were −1.17 V, −8.57 V, −28.76 V and −3.67 V for pristine, Li 1 mol%, Li 10 mol% and Li 15 mol%, respectively. Also, the relation between the field effect mobility and the charge density of Li-doped ZnO semiconductors corresponding to various doping concentrations is shown in Fig. 6b. The increased charge density in the channel layer was ascribed to electrons induced from shallow donors.[35] When more than 10 mol% of Li was added in ZnO semiconductors, V_{on} was increased and it also implied that the addition of Li beyond 10 mol% decreases the charge density of the ZnO semiconductor.

In general silicon semiconductor TFTs, the increment of dopant concentration could degrade the carrier mobility because of impurity scattering. However, in metal oxide semiconductors including ZnO, Hosono *et al.* reported that the mobility increased in proportion to the carrier concentration. This unique characteristic of electron transport for metal oxide semiconductors was induced by potential barriers above the conduction band maximum (CBM).[30] These phenomena have been well explained by Adler's percolation conduction model.[36] In Li-ZnO TFTs, the enhanced field effect mobility was caused by the increment of carrier concentration, which was induced by interstitial Li doping. The increment of carrier concentration could be explained by the optical bandgap shift by Burstein–Moss effects and the turn-on voltage shift.

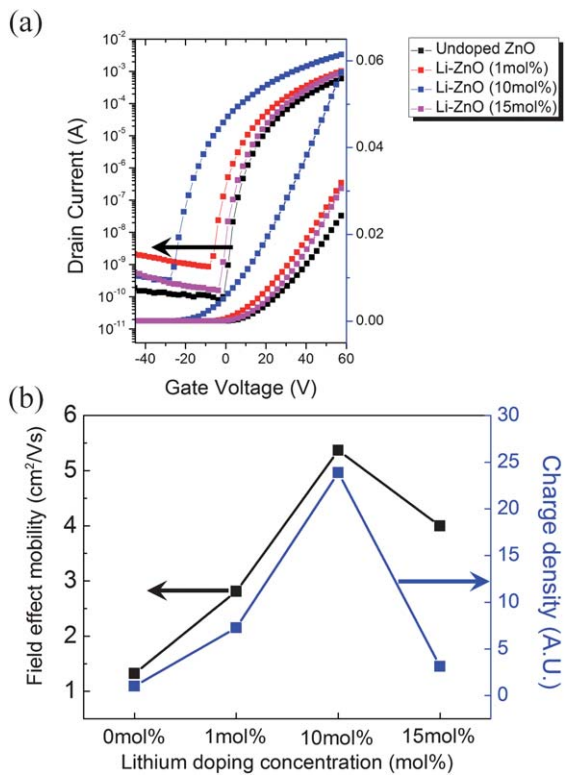

Fig. 6 The average field effect mobility and the charge density of Li-doped ZnO semiconductors with various doping concentrations (0, 1, 10 and 15 mol%). The distribution chart of Li-ZnO TFTs is shown in Fig. S3.†

The fundamental chemical requirements for any sol–gel solution process for metal oxide semiconductors are a complete reaction and no residuals in the semiconductor films after the reaction.[14] Although solution-processed zinc oxide TFTs using various precursors, including In and Ga, which induce good electrical properties, have been reported, ZnO semiconductors based on sol–gel methods are associated with critical problems, as the completeness of the reaction and the presence of residuals should be solved.[37,38] For the complete removal of carbon-based organic ligands such as acetate functional groups in the sol–gel precursors of ZnO semiconductors, these films, coated using ZnO precursors with carbon-based organic ligands, should be fabricated by post-heating at temperatures in excess of 400 °C so as to be residual-free.[39] This high annealing temperature restricts the use of typical plastic and flexible substrates for advanced electronics and is not applicable to the fabrication of low-cost devices. In general, several methods of preparing precursors to overcome high processing temperatures have been reported, but they require an indium dopant for high-performance ZnO TFTs.[17,18] Also, these previously reported results are not free of carbon-residuals after a low-temperature annealing process.

In this study, we proposed the ammine-hydroxo zinc complex as a precursor for ZnO semiconductors. Although the sintering temperature in this method was relatively low compared to the sintering temperatures of typical sol–gel methods, at a maximum of 300 °C, the zinc ammonia films could be transformed easily into ZnO semiconductor films which did not contain any residuals as a consequence of the volatile ammonia ligands.[40] The completeness of the chemical reactions at a low processing temperature reinforced the versatility of the solution-processed ZnO TFTs in this approach. Also, alkali metal doping successfully contributed to the enhancement of the electrical properties of ZnO TFTs without any carbon or unfavourable residuals.

Thermal gravimetric analysis (TGA) data show that the NH_3 loss process finished completely below 100 °C (Fig. S4†). In the TGA analysis, the evaporation of NH_3 occurred earlier than that of water. Above 100 °C, the residual nitrogen was negligible. For an in-depth study of residual nitrogen, we used electron spectroscopy for a chemical analysis. Fig. 7 shows the X-ray photoelectron spectroscopy (XPS) spectra of the pristine, Li-doped, and Na-doped ZnO films fabricated with the aqueous ammine-hydroxo zinc complex precursor on SiO_2 substrates annealed at 300 °C. If residual nitrogen existed in the annealed films, a peak at 398.1 eV would have been detected. However, clear peaks around 398.1 eV could not be observed in any case in the ZnO

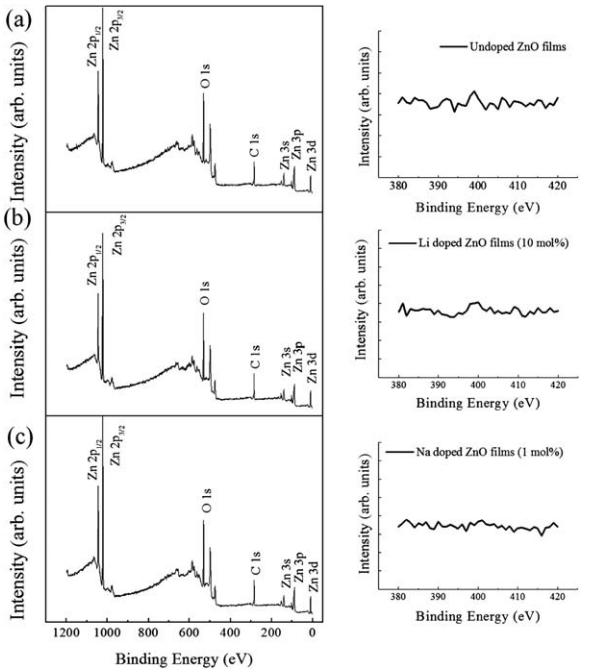

Fig. 7 The wide scan spectrum of ZnO films annealed at 300 °C. (a) Pristine ZnO film. (b) Li-doped ZnO film (10 mol%). (c) Na-doped ZnO film (1 mol%). The right plots show that the residual nitrogen (the peak at 398.1 eV) was not detected.

films. Only alkali metal dopants were detected at 56 eV and 1072 eV for Li and Na, respectively (Fig. S5†). Fig. S6† shows the Li 1s peak located at 52.9 eV which is related to Li interstitials corresponding to the valence state of incomplete oxidation.[41] For detecting alkali metal dopants in ZnO films, we carried out TOF-SIMS (time of flight secondary ion mass spectroscopy). Fig. S7† shows the intensity of Li, Zn and O in alkali metal-doped ZnO thin films. In the Li-ZnO film, high intensity of Li cations was detected. Both XPS and TOF-SIMS showed the existence of alkali metals in alkali metal-doped ZnO films. While investigating the HR-TEM results, an energy-dispersive spectrometer (EDS) was used to assess the Li-doped ZnO films. Fig. S8† shows the EDS spectrum of ZnO films with various Li concentrations (0 mol%, 1 mol%, 10 mol%, and 15 mol%). In the EDS analysis, there were no noticeable spectra of residual nitrogen in the alkali metal-doped ZnO semiconductor films. The investigation of the residuals in alkali metal-doped ZnO semiconductor films, as supported by the XPS and EDS data, showed the completeness of the reaction between the ammine-hydroxo and alkali metal-hydroxo zinc complex as a precursor for ZnO semiconductor films.

3 Conclusions

In summary, high-performance, low-temperature and solution-processed alkali metal-doped ZnO TFTs were introduced in detail and analyzed by HR-TEM, AFM, XPS, EDS, electrical bias stability test and UV-vis spectroscopy. Furthermore, the change in the optical bandgap energy of Li-doped ZnO semiconductor films supported by the Burstein–Moss theory showed successfully the increase and decrease of the field effect mobility of Li-doped ZnO TFTs related to the doping concentrations. From the HR-TEM analysis, we observed that the structures of all of the solution-processed Li-doped ZnO films are polycrystalline. A strong direct correlation between the morphology or crystallinity of ZnO semiconductor films and the electrical performance was not observed. However, we demonstrated that the optical bandgap energy E_{opt} is correlated with the enhancement of the electron mobility of alkali metal-doped ZnO TFTs. The broadening of the E_{opt} values, which are strongly related to the amount of excited electrons from the Fermi level in the valance band to the conduction band, was observed from the Li-doped ZnO 0 mol% film to the Li-doped ZnO 10 mol% film. The increase in the electron donor concentration was the dominant reason for the enhancement in the electron mobility of the alkali metal-doped ZnO TFTs. Also, doping with alkali metals considerably improved the electrical stability of ZnO TFTs. In high and continuous gate biases (V_G) of 50 V over 6000 seconds, alkali metal (Li)-doped ZnO TFTs showed a highly stable threshold voltage and no degradation in the field effect mobility. The higher activation energies for interface trap creation, which resulted from alkali metal doping in ZnO, reduced the amount of charge trapping sites in the ZnO matrix and led to stable operation of the device. Also, although the processing temperature of this method was lower than the processing temperature of conventional sol–gel methods, ammonia–ZnO as a precursor could be transformed completely into ZnO films which didn't contain any residuals owing to the volatile ammonia ligands. Both XPS and EDS analyses showed that there were no residuals in the alkali metal-doped ZnO films.

In this study, we successfully introduced alkali metal-doped ZnO semiconductors which could facilitate the fabrication of high-performance, low-temperature, solution-processed, and indium-free TFTs for cost-effective and mass-produced TFTs for advanced displays. We believe that an in-depth study of the crystal structure, morphology, and optical bandgap of alkali metal-doped ZnO films makes a great contribution to next-generation high-performance TFTs for flexible, printed and transparent electronics.

4 Experimental

We dissolved 0.08139 g of zinc oxide powder ($ZnO \cdot xH_2O$) [Sigma Aldrich] in 12 ml ammonia water (NH_4OH) [Sigma Aldrich]. Because the ZnO particles could easily be precipitated in a precursor solution at room temperature, to increase the solubility of ammonia water, the precursor solution of ZnO had to be kept in a refrigerator or freezer for 5 hours.[42] Amounts of 0.02395 g, 0.2395 g, and 0.3592 g of lithium hydroxide (LiOH) [Sigma Aldrich] were added to 10 ml of de-ionized water in each case. Then, 0.1 ml of each aqueous lithium hydroxide solution was added to the above-mentioned ammine-hydroxo zinc complex solution of 12 ml. The molar ratios between the lithium hydroxide and the ZnO were 1, 10, and 15 mol%.

A heavily doped Si wafer with a thermally grown SiO_2 layer (thickness ~200 nm, capacitance ~17 nF cm^{-2}) was used as the

gate electrode and the gate dielectric. Prior to spin-coating with an alkali metal-doped ZnO precursor, the Si/SiO_2 wafer was cleaned with acetone and isopropyl alcohol (IPA). After spin-coating with the precursor of alkali metal-doped ZnO at 3000 rpm for 30 s, the films were annealed at 300 °C for 1 hour. All source/drain electrodes (100 nm) were then thermally deposited through a shadow mask. The channel length (L) and width (W) were 50 and 1000 μm, respectively.

The thickness of the ZnO thin film and the surface morphology were characterized by a cross-section field emission scanning electron microscope (FE-SEM; S-4800: Hitachi) and an atomic force microscope (AFM; XE150: PSIA). For the optical bandgap, the transmittance of ZnO was measured by a UV-visible spectrometer (Lambda 35: PerkinElmer). HR-TEM (JEM-2100F) was used for the investigation of the Li-doped ZnO crystal structure. To observe the residual nitrogen in the alkali metal-doped ZnO films, XPS (SIGMA PROBE: ThermoVG) and HR-TEM EDS were used.

Acknowledgements

This work was supported by the Basic Research Program (2011-0018113) and the Center for Advanced Soft Electronics under the Global Frontier Research Program (2011-0031635) of the National Research Fund (NRF) funded by the Korean government (MEST). Also, this work was supported by the academy-industry the bilateral collaboration program of LG Display.

References

1 G. H. Gelinck, H. E. A. Huitema, E. Van Veenendaal, E. Cantatore, L. Schrijnemakers, J. B. P. H. Van der Putten, T. C. T. Geuns, M. Beenhakkers, J. B. Giesbers, B. H. Huisman, E. J. Meijer, E. M. Benito, F. J. Touwslager, A. W. Marsman, B. J. E. Van Rens and D. M. De Leeuw, *Nat. Mater.*, 2004, **3**, 106–110.
2 M. Grundmann, H. Frenzel, A. Lajn, M. Lorenz, F. Schein and H. von Wenckstern, *Phys. Status Solidi A*, 2010, **207**, 1437–1449.
3 U. Ozgur, Y. I. Alivov, C. Liu, A. Teke, M. A. Reshchikov, S. Dogan, V. Avrutin, S. J. Cho and H. Morkoc, *J. Appl. Phys.*, 2005, **98**, 041301.
4 H. Frenzel, A. Lajn, H. von Wenckstern, M. Lorenz, F. Schein, Z. P. Zhang and M. Grundmann, *Adv. Mater.*, 2011, **23**, 1424.
5 S. Masuda, K. Kitamura, Y. Okumura, S. Miyatake, H. Tabata and T. Kawai, *J. Appl. Phys.*, 2003, **93**, 1624–1630.
6 P. F. Carcia, R. S. McLean, M. H. Reilly and G. Nunes, *Appl. Phys. Lett.*, 2003, **82**, 1117–1119.
7 J. Zhu, H. Chen, G. Saraf, Z. Duan, Y. Lu and S. T. Hsu, *J. Electron. Mater.*, 2008, **37**, 1237–1240.
8 S. J. Lim, J. M. Kim, D. Kim, S. Kwon, J. S. Park and H. Kim, *J. Electrochem. Soc.*, 2010, **157**, H214–H218.
9 E. Fortunato, P. Barquinha, A. Pimentel, L. Pereira, G. Goncalves and R. Martins, *Phys. Status Solidi RRL*, 2007, **1**, R34–R36.
10 K. Nomura, H. Ohta, A. Takagi, T. Kamiya, M. Hirano and H. Hosono, *Nature*, 2004, **432**, 488–492.
11 J. S. Park, W. J. Maeng, H. S. Kim and J. S. Park, *Thin Solid Films*, 2012, **520**, 1679–1693.
12 D. H. Lee, Y. J. Chang, G. S. Herman and C. H. Chang, *Adv. Mater.*, 2007, **19**, 843.
13 H. C. Huang and T. E. Hsieh, *Nanotechnology*, 2010, **21**, 295707.
14 S. T. Meyers, J. T. Anderson, C. M. Hung, J. Thompson, J. F. Wager and D. A. Keszler, *J. Am. Chem. Soc.*, 2008, **130**, 17603–17609.
15 S. Y. Park, B. J. Kim, K. Kim, M. S. Kang, K. H. Lim, T. I. Lee, J. M. Myoung, H. K. Baik, J. H. Cho and Y. S. Kim, *Adv. Mater.*, 2012, **24**, 834.
16 K. Kim, S. Park, J. B. Seon, K. H. Lim, K. Char, K. Shin and Y. S. Kim, *Adv. Funct. Mater.*, 2011, **21**, 3546–3553.
17 M. G. Kim, M. G. Kanatzidis, A. Facchetti and T. J. Marks, *Nat. Mater.*, 2011, **10**, 382–388.
18 K. K. Banger, Y. Yamashita, K. Mori, R. L. Peterson, T. Leedham, J. Rickard and H. Sirringhaus, *Nat. Mater.*, 2011, **10**, 45–50.
19 L. Zhang, J. Li, X. W. Zhang, X. Y. Jiang and Z. L. Zhang, *Appl. Phys. Lett.*, 2009, **95**, 072112.
20 J. Kim, S. H. Lim and Y. S. Kim, *J. Am. Chem. Soc.*, 2010, **133**, 14721.
21 K. Nomura, H. Ohta, K. Ueda, T. Kamiya, M. Hirano and H. Hosono, *Science*, 2003, **300**, 1269–1272.
22 J. Lee, S. Cha, J. Kim, H. Nam, S. Lee, W. Ko, K. L. Wang, J. Park and J. Hong, *Adv. Mater.*, 2011, **23**, 4183.
23 G. Adamopoulos, A. Bashir, S. Thomas, W. P. Gillin, S. Georgakopoulos, M. Shkunov, M. A. Baklar, N. Stingelin, R. C. Maher, L. F. Cohen, D. D. C. Bradley and T. D. Anthopoulos, *Adv. Mater.*, 2010, **22**, 4764.
24 J. C. Park, S. Kim, S. Kim, C. Kim, I. Song, Y. Park, U. I. Jung, D. H. Kim and J. S. Lee, *Adv. Mater.*, 2010, **22**, 5512–5516.
25 R. B. M. Cross and M. M. De Souza, *Appl. Phys. Lett.*, 2006, **89**, 263513.
26 P. T. Liu, Y. T. Chou and L. F. Teng, *Appl. Phys. Lett.*, 2009, **95**, 233504.
27 K. Suemori, S. Uemura, M. Yoshida, S. Hoshino, N. Takada, T. Kodzasa and T. Kamata, *Appl. Phys. Lett.*, 2007, **91**, 192112.
28 K. Park, S. H. Park, E. Kim, J. D. Kim, S. Y. An, H. S. Lim, H. H. Lee, D. H. Kim, D. Y. Ryu, D. R. Lee and J. H. Cho, *Chem. Mater.*, 2010, **22**, 5377–5382.
29 C. H. Park, S. B. Zhang and S. H. Wei, *Phys. Rev. B: Condens. Matter Mater. Phys.*, 2002, **66**, 073202.
30 H. Hosono, *J. Non-Cryst. Solids*, 2006, **352**, 851–858.
31 G. Srinivasan, R. T. R. Kumar and J. Kumar, *J. Sol-Gel Sci. Technol.*, 2007, **43**, 171–177.
32 E. A. Meulenkamp, *J. Phys. Chem. B*, 1998, **102**, 5566–5572.
33 B. E. Sernelius, K. F. Berggren, Z. C. Jin, I. Hamberg and C. G. Granqvist, *Phys. Rev. B: Condens. Matter Mater. Phys.*, 1988, **37**, 10244–10248.
34 S. M. Sze, *Physics of semiconductor devices*, Wiley-Interscience, New York, 1969.
35 N. L. Dehuff, E. S. Kettenring, D. Hong, H. Q. Chiang, J. F. Wager, R. L. Hoffman, C. H. Park and D. A. Keszler, *J. Appl. Phys.*, 2005, **97**, 064505.
36 D. Adler, L. P. Flora and S. D. Senturia, *Solid State Commun.*, 1973, **12**, 9–12.

37 W. H. Jeong, G. H. Kim, H. S. Shin, B. Du Ahn, H. J. Kim, M. K. Ryu, K. B. Park, J. B. Seon and S. Y. Lee, *Appl. Phys. Lett.*, 2010, **96**, 093503.
38 G. H. Kim, W. H. Jeong, B. Du Ahn, H. S. Shin, H. J. Kim, H. J. Kim, M. K. Ryu, K. B. Park, J. B. Seon and S. Y. Lee, *Appl. Phys. Lett.*, 2010, **96**, 163506.
39 M. Ohyama, H. Kozuka and T. Yoko, *Thin Solid Films*, 1997, **306**, 78–85.
40 R. Theissmann, S. Bubel, M. Sanlialp, C. Busch, G. Schierning and R. Schmechel, *Thin Solid Films*, 2011, **519**, 5623–5628.
41 J. G. Lu, Y. Z. Zhang, Z. Z. Ye, Y. J. Zeng, H. P. He, L. P. Zhu, J. Y. Huang, L. Wang, J. Yuan, B. H. Zhao and X. H. Li, *Appl. Phys. Lett.*, 2006, **89**, 112113.
42 J. J. Richardson and F. F. Lange, *Cryst. Growth Des.*, 2009, **9**, 2570–2575.